



Collaborating with GANIL: Advances in the experimental studies of the ^{46}Mn β^+ decay channel for Nuclear Astrophysics

D. Godos-Valencia^{1,5,*}, L. Acosta^{1,6}, P. Ascher², B. Blank², J. Giovinazzo²,
F. de Oliveira³, C. Fougères⁴, A.M. Sánchez-Benítez⁵.

¹*Instituto de Física UNAM, Mexico;* ²*LP2i-Bordeaux, France;* ³*GANIL, France;*

⁴*CEA/DAM, France;* ⁵*CEAFMC Universidad de Huelva, Spain,*

⁶*Instituto de Estructura de la Materia, CSIC, Spain.*

(^{*}dgodosv@gmail.com)



First ASTRANUCAP Workshop
November 18-19, 2024

⁴⁴Ti relevance in Astrophysics

^{44}Ti nucleosynthesis

- ^{44}Ti and its eventual decay chain is produced in type II supernovae (CCSN). The γ photons emitted during the decay chain (67.9, 78.4, 1157 keV) are observed by telescopes for gamma-astronomy (i.e. INTEGRAL), making ^{44}Ti a good tracer for SN events.
 - ^{44}Ti abundance is quite sensitive to the $^{45}\text{V}(\text{p},\gamma)^{46}\text{Cr}$ reaction rate: the higher the reaction rate, the smaller the ^{44}Ti abundance (L.-S. The, et. al., ApJ 504, 500-515 (1998)).

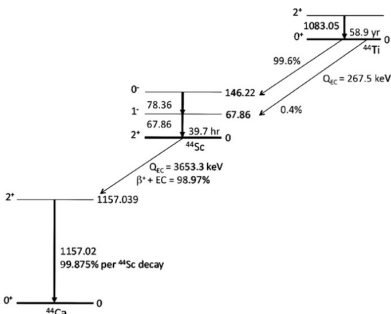


Figura: L.-S. The, et. al., ApJ 504, 500-515
(1998).

Objectives

- To explore unknown excited states of ^{46}Cr , by means of the β^+ -decay of the ^{46}Mn .
- Obtain the energy of new resonant contribution(s) to the $^{45}\text{V}(p,\gamma)^{46}\text{Cr}$ reaction due to new excited state(s) of ^{46}Cr .

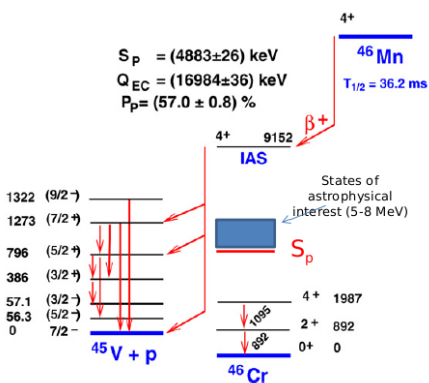


Figura: C. Dossat, et. al., Nucl. Phys. A 792, 18-86 (2007).

β -delayed proton emission

β -delayed proton emission

β -delayed proton emission of ^{46}Mn Decay allows us to seek excited states of the daughter nucleus ^{46}Cr and thus, is an indirect method for measuring resonant contributions to the reaction rate of $^{45}\text{V}(\text{p},\gamma)^{46}\text{Cr}$. (That allows us to study the inverse reaction without building a ^{45}V target for populating $^{46}\text{Cr}^*$ states).

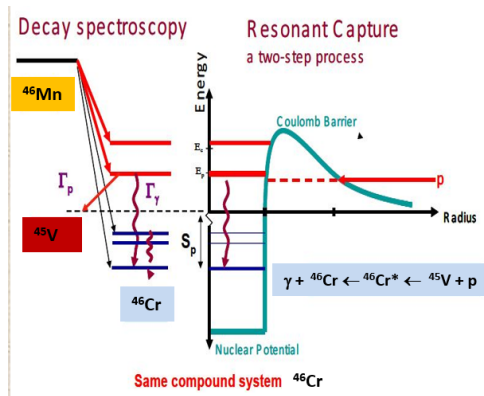
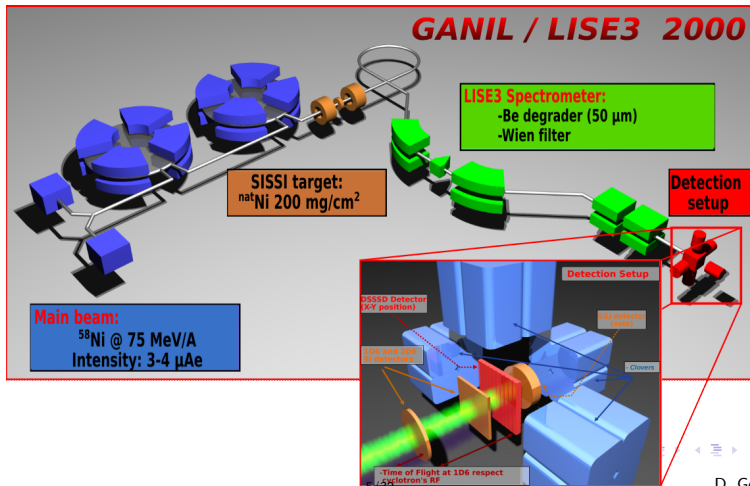


Figura: Adapted from L. Trache, et. al., AIP Conf. Proc 1409-1, 67-70 (2011).

Beam production at LISE@GANIL for E666 experiment

Data was taken from the experiment “Isospin mixing in pf-shell proton emitters” (Code: E666, Spokesperson: Bertram Blank, from CEN-BG, France) developed using the fragment separator LISE@GANIL (Caen, France).



Experimental analysis

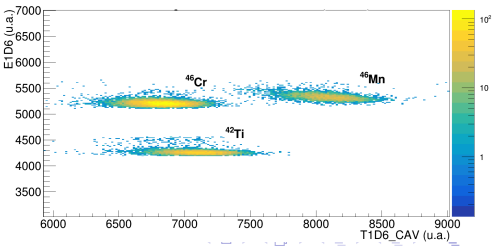
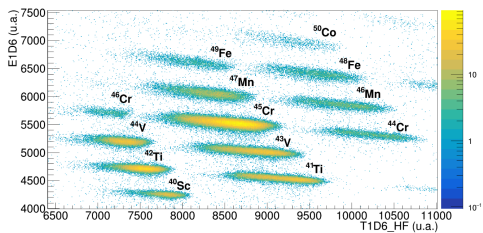
1. As a first step calibrations for the DSSSD X & Y strips, and for the HPGe clover sections were performed.
 - 1.1 For the DSSSD, a triple α -source (^{239}Pm , ^{241}Am y ^{244}Cm) was used.
 - 1.2 For the HPGe clovers, we use $^{56+60}\text{Co}$, ^{207}Bi , and $^{133}\text{Ba} + ^{137}\text{Cs}$ sources.
2. Later, the ions of interest were selected, ^{46}Mn , by means of Energy loss vs Time of Flight (ToF) 2D histograms.
3. Finally, decay events corresponding to the ^{46}Mn were identified using spatial and time correlations between the implantation and the decay signals.



Experimental analysis

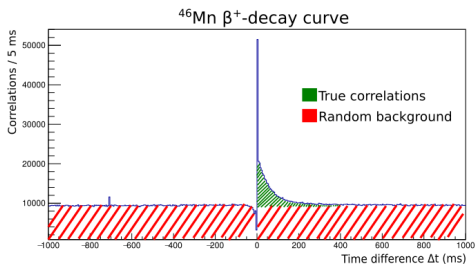
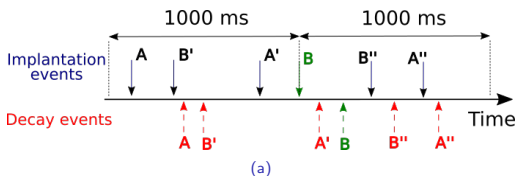
^{46}Mn identification

- We use the Time of Flight (ToF) in the 1D6 detector to identify the isotope of interest, ^{46}Mn , among others.
- These events were selected using graphical cut filters, one for the ToF with respect to the High-Frequency Signal of the Cyclotron (top figure) and the other with respect to the time given by CAVIAR detector (bottom figure). More than 3.15×10^5 events of ^{46}Mn were selected during approximately 71.5 hrs of data acquisition.



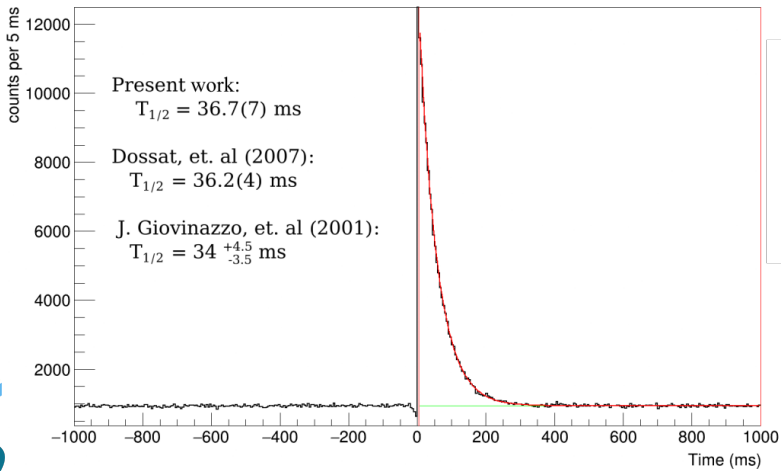
Time-correlated events

The time correlations between the ^{46}Mn implantation events and the decay ones were established in the following way:

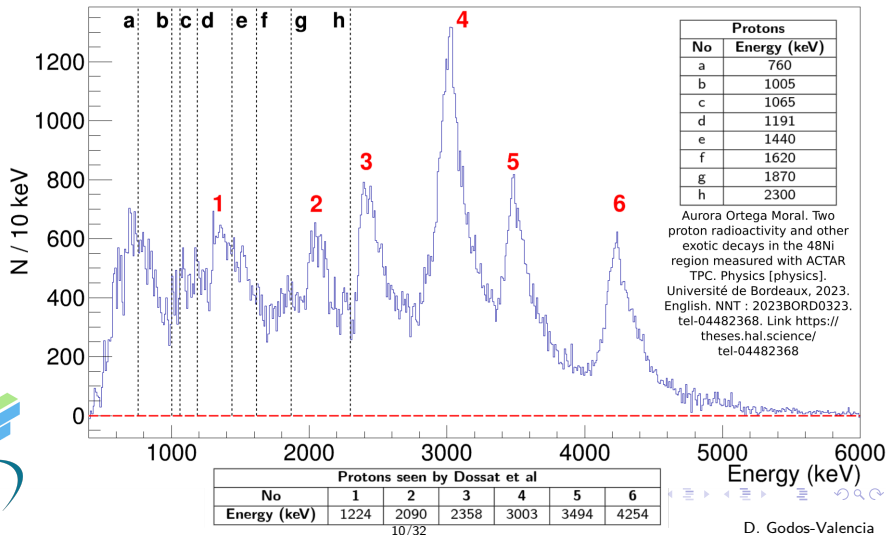


^{46}Mn β -decay curve

The half-life was obtained applying a $E > 1500$ keV filter and the systematic error was set as the difference between this value and the one with a $E > 1000$ keV filter.



β -delayed proton energy spectra



Efficiency evaluation for β and γ detection

γ detection efficiency of HPGe clovers

- The peaks of the γ -calibration sources were used: $^{56+60}\text{Co}$, ^{207}Bi , and $^{133}\text{Ba} + ^{137}\text{Cs}$.
- The efficiency in each peak was found using the equation:

$$\varepsilon_{\gamma} = \frac{N_{\gamma} * \text{Div}}{I_{\gamma} A T_{\text{run}} (1 - \tau)}$$

- Then we fit the following function $f(E) = \exp a + b \ln E$ to get the γ efficiency detection at any energy value.

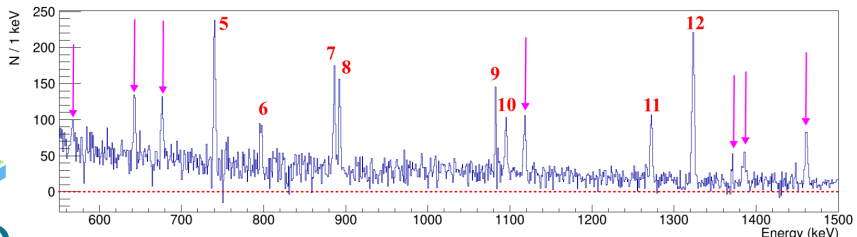
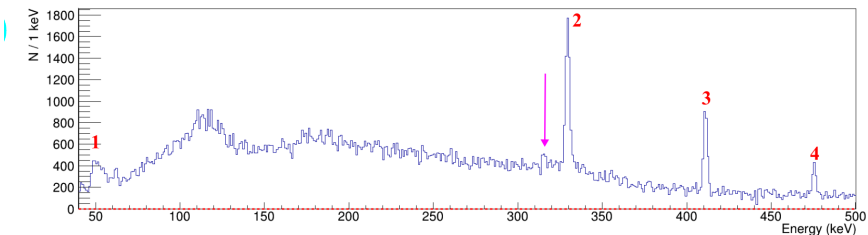
β detection efficiency of DSSSD strips

- We used the decay curves of the pure β emitters: ^{46}Cr and ^{42}Ti (within the cocktail beam).
- While doing the exponential fit, the total number of detected by the DSSSD strips N_{β} was counted.
- Then the β detection efficiency was obtained following the equation:

$$\varepsilon_{\beta} = \frac{N_{\beta}}{N_{\text{imp}} (1 - \tau)}$$



β -delayed γ energy spectra



Peak intensities

Measuring $\beta - \gamma$ intensities

- To measure the $\beta - \gamma$ intensities of the γ peaks we use the equation:

$$I_{\beta,\gamma} = \frac{N_\gamma}{\varepsilon_\beta * \varepsilon_\gamma * N_{\text{imp}} * (1 - \tau)},$$

- where N_γ stands for the number of γ s detected, N_{imp} for the number of implantation events, τ for the dead time, ε_β for the β detection efficiency, and ε_γ for the γ detection efficiency.

Measuring proton- γ intensities

- In the case of the p- γ intensities, we use the equation:

$$I_{p,\gamma} = \frac{N_\gamma}{\varepsilon_p * N_{\text{imp}} * (1 - \tau)},$$

- where ε_p , the proton detection efficiency, can be considered as 1.



γ -peak intensities

| Gammas | | ^{46}Mn | | | |
|--------|--------------|-------------------------|-------------------------------|--|---------------------------|
| No | Energy (keV) | I _{Dossat} (%) | I _{Present work} (%) | Type | Process |
| 1 | 54.4 | | 0.2(1) | ^{45}V : $5/2^-$ to $7/2^-$ | $\text{I}_{p,\gamma}$ |
| 2 | 329.4 | 11.3(11) | 6.4(2) | ^{45}V : $3/2^+$ to $3/2^-$ | $\text{I}_{p,\gamma}$ |
| 3 | 410.2 | 6.7(7) | 4.4(3) | ^{45}V : $5/2^+$ to $3/2^+$ | $\text{I}_{p,\gamma}$ |
| 4 | 475.2 | 1.7(5) | 1.9(2) | ^{45}V : $7/2^+$ to $5/2^+$ | $\text{I}_{p,\gamma}$ |
| 5 | 739.7 | 2.4(8) | 2.0(1) | ^{45}V : $5/2^+$ to $5/2^-$? | $\text{I}_{p,\gamma}$ |
| 6 | 796.1 | 1.6(4) | 1.8(5) | ^{45}V : $5/2^+$ to $7/2^-$? | $\text{I}_{p,\gamma}$ |
| 7 | 885.7 | 2.2(7) | 1.3(5) | ^{45}V : $7/2^+$ to $3/2^+$? | $\text{I}_{p,\gamma}$ |
| 8 | 892.5 | 25(6) | 30(6) | ^{46}Cr : 2^+ to 0^+ | $\text{I}_{\beta,\gamma}$ |
| 9 | 1094.7 | 26(7) | 24(6) | ^{46}Cr : 4^+ to 2^+ | $\text{I}_{\beta,\gamma}$ |
| 10 | 1118.0 | 1.5(10) | 1.1(2) | ^{45}V : $9/2^+$ to $5/2^+$? | $\text{I}_{p,\gamma}$ |
| 11 | 1272.6 | 3.5(5) | 1.4(1) | ^{45}V : $7/2^+$ to $7/2^-$ | $\text{I}_{p,\gamma}$ |
| 12 | 1322.1 | 4.9(11) | 2.8(1) | ^{45}V : $9/2^-$ to $7/2^-$ | $\text{I}_{p,\gamma}$ |



Proton-peak intensities

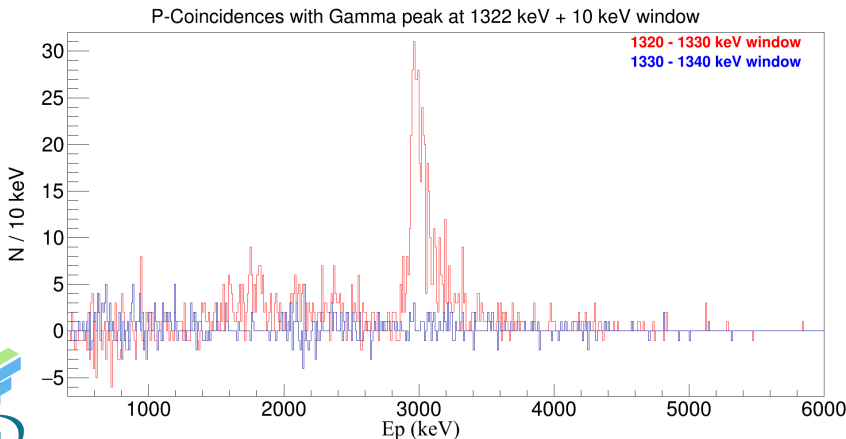
To calculate the proton-peak intensities we use that $I_p = N_p / (N_{\text{imp}} * (1 - \tau))$

| Protons | | ^{46}Mn | | |
|---------|--------------|--------------------------|-----------------------------|---|
| No | Energy (keV) | $I_{\text{Dossat}} (\%)$ | $I_{\text{This work}} (\%)$ | Process |
| 1 | 1224 | 1.8(3) | 0.1(5) | ? \downarrow ? |
| 2 | 2090 | | 1.8(3) | decay of ^{45}Cr ? |
| 3 | 2358 | 1.7(4) | 5.0(3) | ^{46}Cr IAS to $^{45}\text{V}^{9/2+}$? |
| 4 | 3003 | 6.5(9) | 8.8(3) | ^{46}Cr IAS to $^{45}\text{V}^{7/2+}$ |
| 5 | 3494 | 3.5(6) | 4.4(2) | ^{46}Cr IAS to $^{45}\text{V}^{5/2+}$ |
| 6 | 4254 | 5.5(9) | 3.8(1) | ^{46}Cr IAS to $^{45}\text{V}^{\text{gs}}$ |

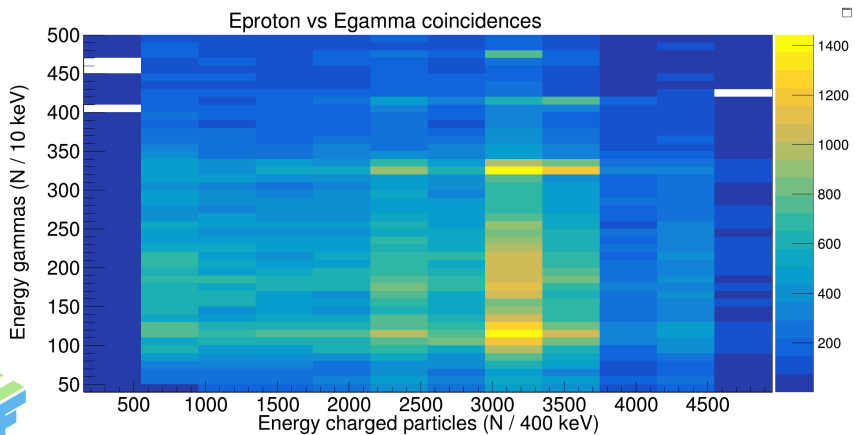


p- γ coincidences

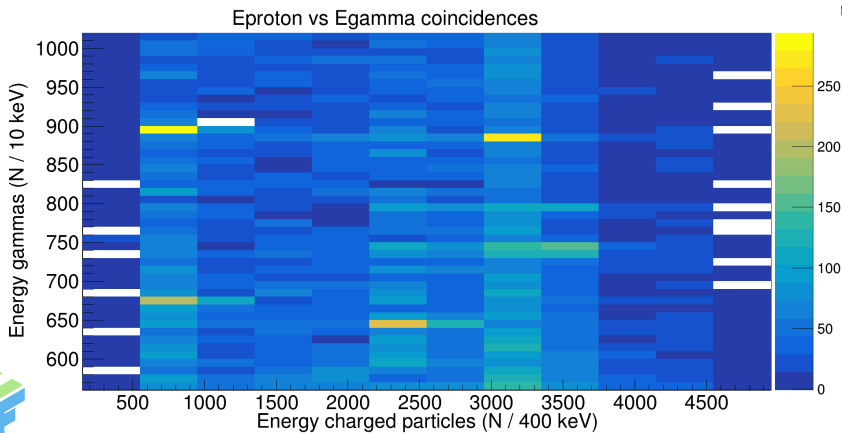
We also studied the p- γ coincidences by applying selection windows for the gamma peaks in the proton energy spectrum:



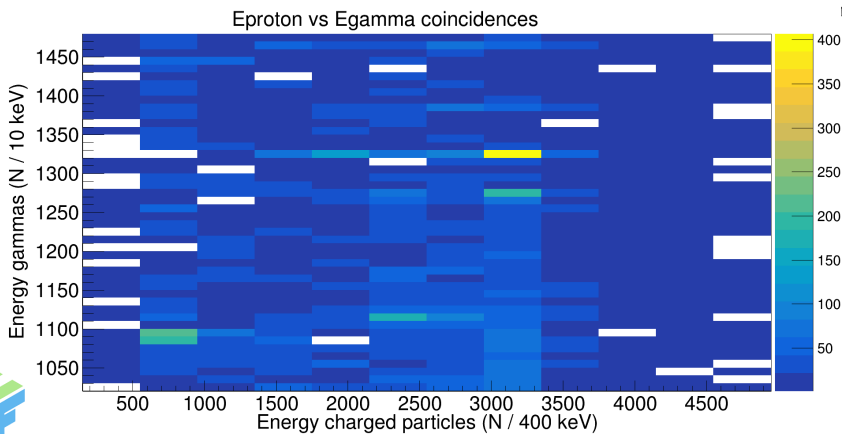
p- γ coincidences for 40-500 keV γ 's



p- γ coincidences for 550-1020 keV γ 's

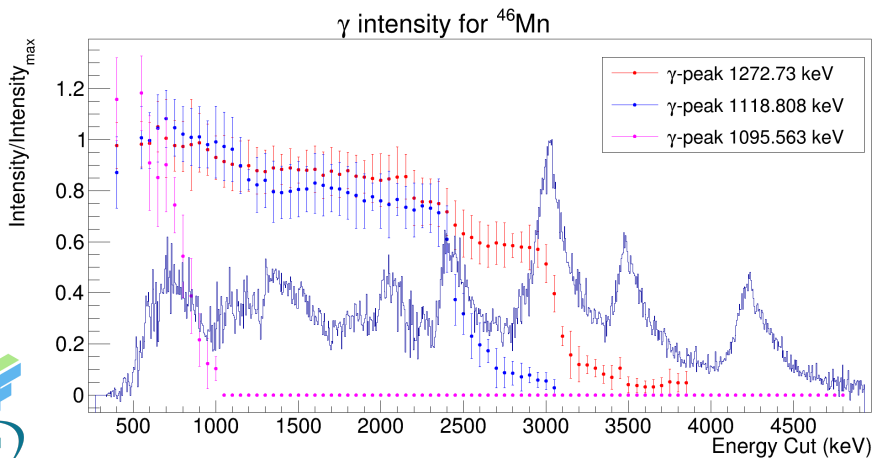


p- γ coincidences for 1020-1480 keV γ 's



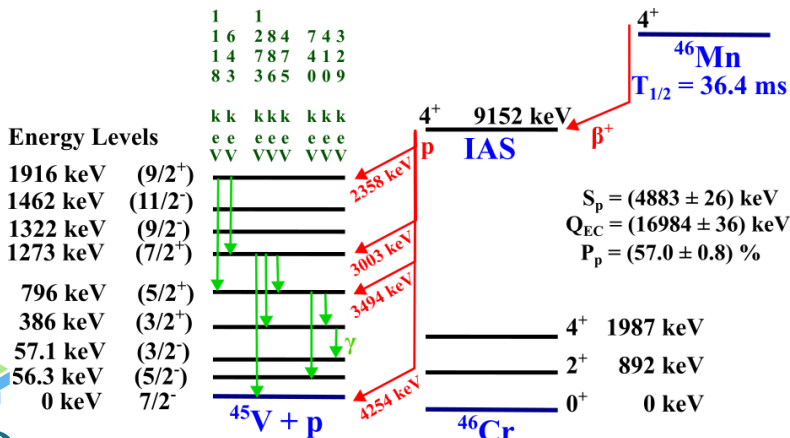
p- γ coincidences

Another way to see the p- γ coincidences was by applying energy thresholds for the minimum proton energy in the γ energy spectrum:



p- γ coincidences

With the information of the p- γ coincidences we could draw the following decay scheme:



Conclusions and future work

- The ^{46}Mn β -decay curve and therefore its half-life was obtained. The half-life is compatible with previous results from the literature.
- Energy spectra for protons (400-6000 keV) and γ photons (40-500 keV and 550-1500 keV) related to the ^{46}Mn β -decay were also obtained. Those spectra are also compatibles with J. Giovinazzo, et al. and Dossat, et al. results, **with greater statistic than either two publications**.
- The decay curves of pure β emitters, ^{42}Ti and ^{46}Cr , were analyzed also obtaining the β detection efficiency. Discrepancies with the literature are being analized.
- Next steps of the analysis:
 1. To further analyze the p- γ correlations in order to identify which γ peak its emitted at a specific proton energy.
 2. To apply Shell Model, also looking into the mirror nuclei ^{46}Ti , to have a list of possible excited states.



Acknowledgments

- This work is partially supported by DGAPA-UNAM IG101423 and CONACyT 314857 projects.
- We thank support from Centro de Estudios Avanzados en Física, Matemáticas y Computación of the University of Huelva CEAFMC-UHU.
- Special thanks to **ASTRANUCAP** organizers for making this talk possible.



- Table obtained from L.-S. The, et. al., ApJ 504, 500-515 (1998).

TABLE 5

ORDER OF IMPORTANCE OF REACTIONS PRODUCING ^{44}Ti AT $n = 0^*$

| Reaction | Slope |
|--|--------|
| $^{44}\text{Ti}(\alpha, p)^{47}\text{V}$ | -0.394 |
| $\alpha(2x, \gamma)^{12}\text{C}$ | +0.386 |
| $^{45}\text{V}(p, \gamma)^{46}\text{Cr}$ | -0.361 |
| $^{40}\text{Ca}(\alpha, \gamma)^{44}\text{Ti}$ | +0.137 |
| $^{57}\text{Co}(p, \eta)^{57}\text{Ni}$ | +0.102 |
| $^{36}\text{Ar}(x, p)^{39}\text{K}$ | +0.037 |
| $^{44}\text{Ti}(\alpha, \gamma)^{48}\text{Cr}$ | -0.024 |
| $^{12}\text{C}(\chi, \gamma)^{16}\text{O}$ | -0.017 |
| $^{57}\text{Ni}(p, \eta)^{58}\text{Cu}$ | +0.013 |
| $^{58}\text{Cu}(p, \gamma)^{59}\text{Zn}$ | +0.011 |
| $^{36}\text{Ar}(\chi, \gamma)^{40}\text{Ca}$ | +0.008 |
| $^{44}\text{Ti}(p, \eta)^{45}\text{V}$ | -0.005 |
| $^{57}\text{Co}(p, \eta)^{58}\text{Ni}$ | +0.002 |
| $^{57}\text{Ni}(\alpha, \gamma)^{58}\text{Cu}$ | +0.002 |
| $^{54}\text{Fe}(\chi, \gamma)^{57}\text{Ni}$ | +0.002 |
| $^{40}\text{Ca}(x, p)^{43}\text{Sc}$ | -0.002 |

^a Order of importance of reactions producing ^{44}Ti at $\eta = 0$ according to the slope of $X(^{44}\text{Ti})$ near the standard reaction rates.

Sensitivity of ^{44}Ti and ^{56}Ni Production in Core-collapse Supernova Shock-driven Nucleosynthesis to Nuclear Reaction Rate Variations

Shiv K. Subedi¹, Zach Meisel¹, and Grant Merz¹

Institute of Nuclear & Particle Physics, Department of Physics & Astronomy, Ohio University, Athens, OH 45701, USA; ss383615@ohio.edu, meisel@ohio.edu

Received 2020 February 25; revised 2020 May 16; accepted 2020 May 26; published 2020 July 16

Abstract

Recent observational advances have enabled high resolution mapping of ^{44}Ti in core-collapse supernova (CCSN) remnants. Comparisons between observations and models provide stringent constraints on the CCSN mass. However, past work has identified several uncertain nuclear reaction rates that influence ^{44}Ti and ^{56}Ni production in postprocessing model calculations. We evaluate one-dimensional models of $15M_{\odot}$, $18M_{\odot}$, $22M_{\odot}$, and $25M_{\odot}$ stars from zero age main sequence through CCSN using Modules for Experiments in Stellar Astrophysics and investigate the previously identified reaction rate sensitivities of ^{44}Ti and ^{56}Ni production. We tested the robustness of our results by making various assumptions about the CCSN explosion energy and metal cut. We found a number of reactions that have a significant impact on the nucleosynthesis of ^{44}Ti and ^{56}Ni , particularly for lower progenitor masses. Notably, the reaction rates of $\text{Fe}^{56}(\text{e}^+, \nu)\text{Fe}^{57}$, $\text{Fe}^{56}(\text{e}^-, \bar{\nu})\text{Fe}^{55}$, $\text{Fe}^{56}(\text{e}^+, \nu)\text{Co}^{57}$, $\text{Ni}^{60}(\text{e}^+, \nu)\text{Cu}^{61}$, $\text{Ni}^{60}(\text{e}^-, \bar{\nu})\text{Co}^{59}$, $\text{Co}^{59}(\text{e}^+, \nu)\text{Cr}^{58}$, $\text{Co}^{59}(\text{e}^-, \bar{\nu})\text{Ni}^{60}$, $\text{Co}^{59}(\text{e}^+, \nu)\text{Ni}^{61}$, and $\text{Co}^{59}(\text{e}^-, \bar{\nu})\text{Ni}^{60}$ were found to have the largest impact on the final yields.

- Not $^{45}\text{V}(\text{p},\gamma)^{46}\text{Cr}$, but $^{47}\text{V}(\text{p},\gamma)^{48}\text{Cr}$!
 - $^{39}\text{K}(\text{p},\gamma)^{40}\text{Ca}$ and $^{39}\text{V}(\text{p},\alpha)^{36}\text{Ar}$ also affect ^{44}Ti abundancy.

- ^{44}Ti is produced when a shock-wave after the core-collapse reaches the α -rich region in the cooling phase ($1 < T_9 < 5$).

- As $\vec{J} = \vec{\ell} + \vec{j}_1 + \vec{j}_2$ and $\Pi = \pi_1 \pi_2 (1)^{-\ell}$, for $^{45}\text{V} + \text{p} \rightarrow ^{46}\text{Cr}^*$ and only considering $\ell = 0, 1$ resonant capture then the candidates for resonances are:

$$J^\pi(^{45}\text{V}_{\text{gs}}) = 7/2^-; \quad J^\pi(\text{p}) = 1/2^+ \Rightarrow J^\pi(^{45}\text{V}_{\text{gs}}) = 2^+, 3^+, 4^+, 5^+, 3^-, 4^-$$

- On the other hand, allowed β -decay transitions follows:

$$\Delta J = 0; \quad \pi_i = \pi_f \quad \text{for Fermi}$$

$$\Delta J = 0, 1; \quad \pi_i = \pi_f \quad \text{for Gamow-Teller}$$

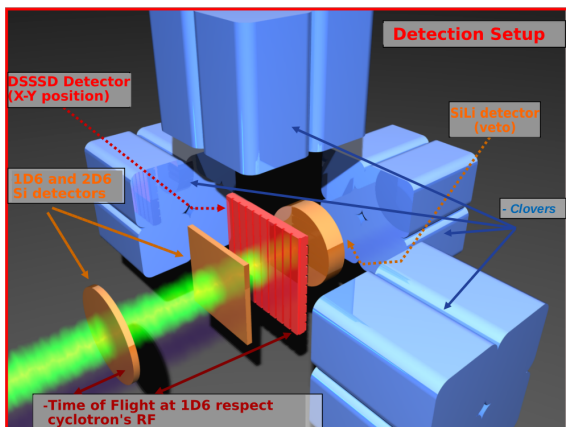
As $J^\pi(^{46}\text{Mn}_{\text{gs}}) = 4^+$ and considering only allowed transitions:

$J^\pi(^{46}\text{Cr}^*) = 3^+, 4^+, 5^+$ ($2^+, 3^-$ and 4^- could be sufficiently populated but they are strongly inhibited).



Detection setup

- The primary beam was a $^{58}\text{Ni}^{26+}$ at 74.5 MeV/u, which collided with a 230.6 mg/cm² thick $^{\text{nat}}\text{Ni}$ target.
- With the LISE separator elements, the isotopes to be implanted in the detectors array were selected.
- The detectors array used during the experiment is shown:

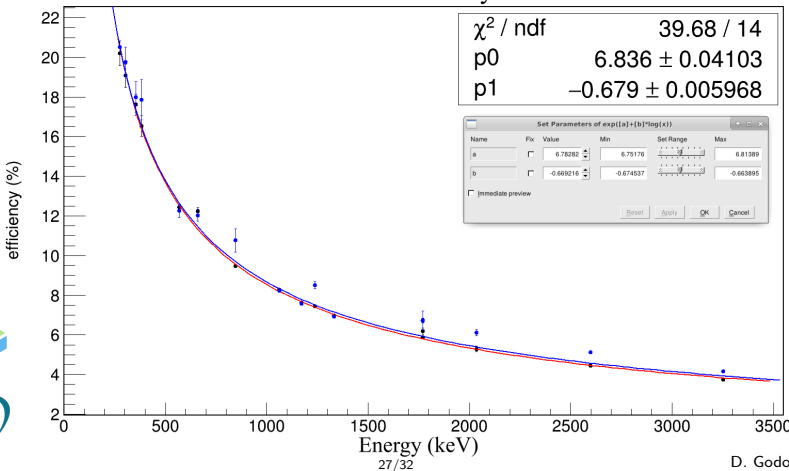


Gamma efficiency curve

The gamma efficiency curve obtained for the analysis is shown in the next figure:

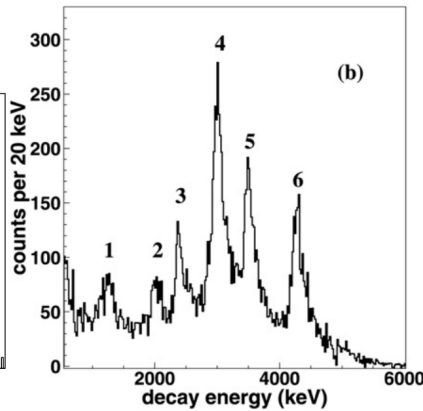
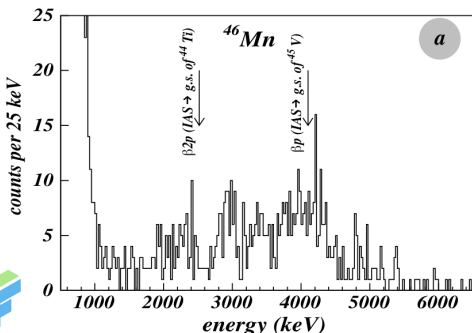
:

Gamma efficiency curve



Charged particle spectra

The charged particle spectra obtained by Dossat and Giovinazzo are presented:



(c)

(d)

Detectores de partículas cargadas. Detectores Si y SiLi

1. Los detectores identificados por los nombres 1D6 y 2D6 se usaron como ΔE . La energía depositada en estos detectores depende de Z, A y la velocidad de la partícula incidente y se describe por medio de la ecuación de Bethe-Bloch.
2. El SiLi fue usado para detener los fragmentos del haz que no se hubieran detenido en los detectores previos. También fue usado como Veto para descartar isótopos de ^{46}Mn que no fueron implantados en el DSSSD.
3. El 1D6 cuenta con un grosor de $300\ \mu\text{m}$; mientras que el 2D6 tiene un grosor de $297\ \mu\text{m}$ y el SiLi de $500\ \mu\text{m}$.



Detectores de partículas cargadas. Detector DSSSD

El **Double-Sided Si Strip Detector** (DSSSD) se compone de dos placas divididas en secciones P y N, las cuales están a su vez divididas en 16 tiras o Strips (unas vertical y otras horizontalmente). La información de las señales de las tiras X-Y se pueden usar para formar una cuadrícula en la etapa de procesamiento de datos; cada píxel de la cuadrícula corresponde a un cuadro de $3 \times 3 \text{ mm}^2$ de área. El DSSSD tiene un grosor de $316 \mu\text{m}$.

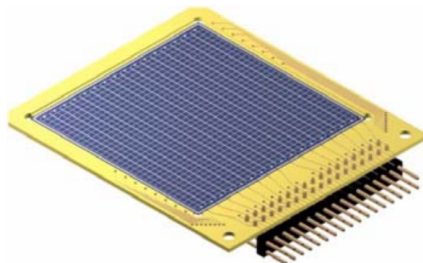
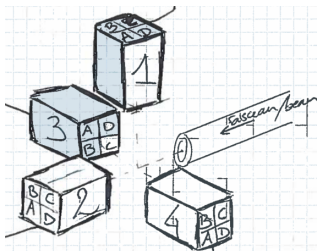


Figura: O. Tengblad, Nucl. Instrum. Methods. Phys. Res. B, 525:3, 458-464, (2004)

Detectores de fotones γ

El sistema de detección de fotones se compone por 4 clovers etiquetados del 1 al 4 para su distinción. Éstos, a su vez, se dividen en 4 secciones denotadas por las letras A, B, C, D. Cada sección del clover consiste en un cristal altamente puro de Ge (HPGe).



(a)



(b)

Adquisición de datos

Se tienen varias señales de trigger (1D6, 2D6, DSSSD y SiLi). En caso de que alguna de ellas se dispare, se almacenan los datos de todos los detectores junto con los triggers disparados en un vector concreto para cada suceso. En total el DSSSD produce unas 32 señales, las cuales deben ser rescatadas por el DAQ.

Señales

